



Novel 6-aminofuro[3,2-c]pyridines as potent, orally efficacious inhibitors of cMET and RON kinases

Arno G. Steinig^{a,*}, An-Hu Li^{a,*}, Jing Wang^a, Xin Chen^a, Hanqing Dong^a, Caterina Ferraro^a, Meizhong Jin^a, Mridula Kadalbajoo^a, Andrew Kleinberg^a, Kathryn M. Stolz^a, Paula A. Tavares-Greco^a, Ti Wang^a, Mark R. Albertella^a, Yue Peng^a, Linda Crew^a, Jennifer Kahler^a, Julie Kan^a, Ryan Schulz^a, Andy Cooke^b, Mark Bittner^b, Roy W. Turton^b, Maryland Franklin^b, Prafulla Gokhale^b, Darla Landfair^b, Christine Mantis^b, Jen Workman^b, Robert Wild^b, Jonathan Pachter^a, David Epstein^a, Mark J. Mulvihill^a

^a OSI Pharmaceuticals, LLC, A Wholly-Owned Subsidiary of Astellas US, 1 Bioscience Park Drive, Farmingdale, NY 11735, USA

^b OSI Pharmaceuticals, LLC, A Wholly-Owned Subsidiary of Astellas US, 2860 Wilderness Place, Boulder, CO 80301, USA

ARTICLE INFO

Article history:

Received 27 March 2013

Revised 20 May 2013

Accepted 21 May 2013

Available online 30 May 2013

Keywords:

Furopyridines

Tyrosine kinase inhibitor

Tumor growth inhibition

cMET

RON

ABSTRACT

A series of novel 6-aminofuro[3,2-c]pyridines as kinase inhibitors is described, most notably, OSI-296 (**6**). We discuss our exploration of structure–activity relationships and optimization leading to OSI-296 and disclose its pharmacological activity against cMET and RON in cellular assays. OSI-296 is a potent and selective inhibitor of cMET and RON kinases that shows *in vivo* efficacy in tumor xenografts models upon oral dosing and is well tolerated.

© 2013 Elsevier Ltd. All rights reserved.

2-Aminopyridines **1** are a common chemotype for inhibitors of kinases. Examples include the recently approved ALK/cMET inhibitor Crizotinib (PF-02341066, **2**),¹ AXL/cMET inhibitor **3** first disclosed by AstraZeneca,² and the CHK2 inhibitor **4**.³ Typically, the pyridine nitrogen acts as hydrogen bond acceptor for a backbone NH of the hinge region, while the 2-amino group donates a hydrogen bond to the interior hinge carbonyl,⁴ thus interacting with the same residues as ATP in a mutually exclusive way. The C3 substituent then reaches towards the interior of the kinase, while the C5 substituent projects through a channel towards the solvent-exposed region.⁵ Fusing an additional (hetero)aromatic ring onto the 2-aminopyridine core via its 4- and 5-positions would retain the hinge binding moiety while providing different vectors for substituents to interact with the protein. Herein, we demonstrate this concept with 6-aminofuro[3,2-c]pyridines **5** and disclose the optimization of this series leading to the potent cMET/RON inhibitor OSI-296 (**6**) (Fig. 1).

cMET and RON are receptor tyrosine kinases of the MET proto-oncogene family that share significant sequence and structural

homology.⁶ They are activated by their respective ligands HGF (Hepatocyte Growth Factor) and MSP (Macrophage Stimulating Protein) and signal via the PI3K/AKT and MAPK pathways. Signaling through the cMET/HGF system can be deregulated in cancer by mechanisms such as HGF-dependent autocrine activation, cMET gene amplification, cMET transcriptional upregulation, chromosomal rearrangements, and/or the presence of activating mutations.⁷ Approaches to abrogate aberrant cMET signaling that have led to agents in clinical trials include inhibiting the kinase function of cMET with small molecules and preventing ligand–receptor binding with HGF or cMET antibodies.⁸ While activating mutations or gene amplification of RON in cell lines or tumor samples have not been reported, constitutively active RON variants generated by alternative splicing⁹ or by methylation-dependent promoter usage [short-form RON (sfRON)]¹⁰ have been identified. Cells expressing these RON proteins show greater scatter activity, focus formation, anchorage-independent growth, and tumor formation in nude mice compared with cells expressing wild-type RON, suggesting that activation of RON may contribute to the invasive phenotype of various human carcinomas.^{9,10}

The cellular and *in vivo* component of our cMET drug discovery cascade was built upon the MKN45 human gastric carcinoma cell line. This cancer cell line displays a high level of amplification of

* Corresponding authors. Tel.: +1 845 490 8365 (A.G.S.).

E-mail addresses: arnosteinig@gmail.com (A.G. Steinig), anhu_li@yahoo.com (A.-H. Li).

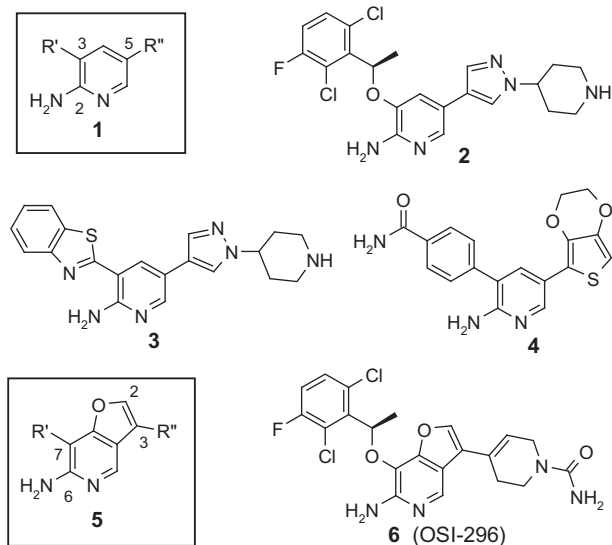
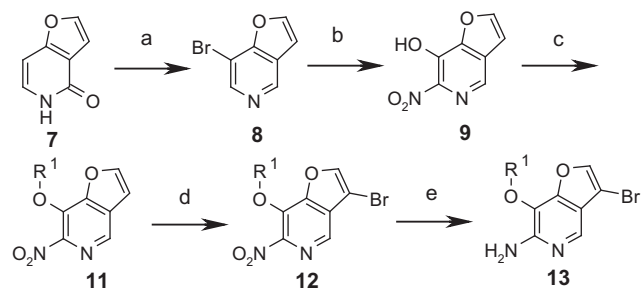


Figure 1. 2-Aminopyridines and 6-aminofuro[3,2-c]pyridines as kinase inhibitors.

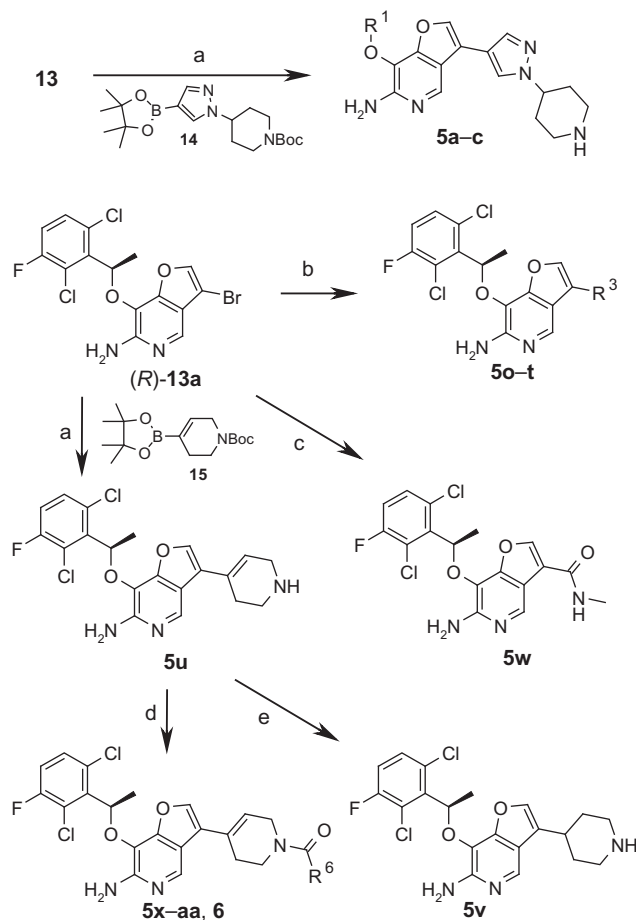


Scheme 1. Synthesis of the furo[3,2-c]pyridine intermediates **12** and **13**. Reagents and conditions: (a) (i) NBS, DMF; (ii) POBr₃, toluene; (iii) sodium formate, Pd(PPh₃)₄, DMF, 100 °C, overnight; (b) (i) Pd₂dba₃, 2-di-*tert*-butylphosphino-3,4,5,6-tetra-methyl-2',4',6'-triisopropyl-1,1'-biphenyl, KOH, dioxane/water 1:1, 100 °C, overnight, (ii) concd HNO₃, 0 °C, 30 min; (c) R¹-OH (**10**), DIAD, PPh₃, THF, 0 °C to rt; (d) (i) Br₂, CCl₄, 50 °C, overnight, (ii) DBU, THF 0 °C, 1 h; (e) Fe powder, cat. HCl, EtOH, 95 °C, 1 h.

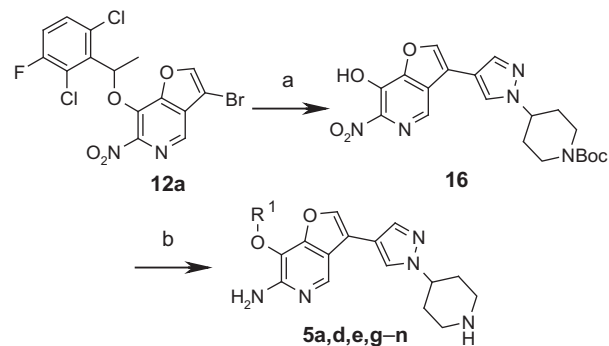
cMET and constitutive activation of cMET and can be used for xenografts in immunocompromised mice. Treatment of this cell line with a selective cMET inhibitor was reported to result in induction of apoptosis and inhibition of proliferation, whereas non-MET-amplified cell lines were not affected.¹¹ This cell line is thus 'driven' by c-MET, and antiproliferative effects correlate with the inhibition of cMET phosphorylation so that the cell proliferation IC₅₀ values¹² can be used as surrogate for the cMET cell mechanistic IC₅₀ values.^{13,14} Cellular activity against RON was assessed in HeLa cells transiently transfected with sfRON, monitoring the endogenous pRON at the autophosphorylation site Y1238/1239.¹⁵

The synthesis of the key furo[3,2-c]pyridine intermediates **12** and **13** is shown in Scheme 1. The furo[3,2-c]pyridinone **7**¹⁶ was converted to the known 7-bromofuro[3,2-c]pyridine (**8**) in three steps by reaction with NBS, treatment with POBr₃, and selective reduction of the 4-Br substituent.¹⁷ Conversion of the 7-Br group to 7-OH and subsequent nitration at C6 provided **9**, onto which the R¹ substituent was introduced by Mitsunobu reaction with the alcohols **10**. Addition of bromine to the furan ring, followed by elimination of HBr with DBU gave intermediate **12**. Subsequent reduction of the nitro group yielded **13**.

Compound **13** served as a versatile intermediate for incorporating substituents at the 3-position of the furo[3,2-c]pyridine core, providing a second point of diversity (Scheme 2). A variety of aryl,

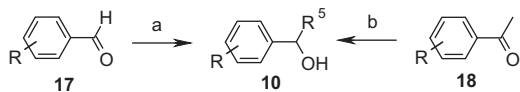


Scheme 2. Synthesis of the furo[3,2-c]pyridines **5** and **6**. Reagents and conditions: (a) (i) Pd(PPh₃)₄, K₂CO₃, dioxane/water or DME/water 4:1, 100 °C; (ii) 4 M HCl in dioxane, rt; (b) (pinacolato)B-R³ or (HO)₂B-R³, Pd(PPh₃)₄, K₂CO₃, dioxane/water or DME/water 4:1, 100 °C; or Bu₃Sn-R³, Pd(PPh₃)₄, KF, dioxane, 100 °C; (c) (i) CO, Pd(PPh₃)₄, DIPEA, MeOH, 68 °C, overnight, (ii) 1 M HCl aq, 100 °C, 7 h, (iii) TBTU, MeNH₂-HCl, DIPEA, DMF, rt, 30 min; (d) R⁶C(=O)Cl or R⁶-NCO or TMS-NCO; (e) H₂, Pd/C, EtOAc, rt, 1 h.



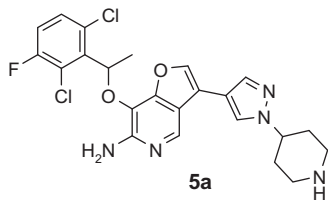
Scheme 3. Alternative synthesis of the furo[3,2-c]pyridines **5**. Reagents and conditions: (a) (i) **14**, Pd(PPh₃)₄, K₂CO₃, dioxane/water 4:1, 100 °C, (ii) 48% aq HBr, 60 °C, overnight, (iii) Boc₂O, NEt₃(iPr)₂, DCM, 0 °C, 1–3 h; (b) (i) R¹-OH (**10**), DIAD, PPh₃, THF, 0 °C to rt, (ii) Fe powder, cat. HCl, EtOH, 95 °C, 1 h; (iii) 4 M HCl in dioxane, rt.

hetaryl, and heterocyclyl substituents could be introduced by Suzuki or Stille coupling, followed in the case of Boc-protected boronates **14**^{1a} and **15** by deprotection with HCl (**5a-c,o-u**). The tetrahydropyridine **5u** thus obtained was subsequently acylated with acid chlorides, chloroformates, carbamoyl chlorides, isocya-



Scheme 4. Synthesis of the alcohols **10**. Reagents and conditions: (a) $R^5\text{MgBr}$ or $R^5\text{MgCl}$, THF; (b) NaBH_4 , EtOH.

Table 1
cMET and RON potencies of **5a**



Compd	cMET biochem. IC_{50} (μM) ¹⁸	cMET cell mech. IC_{50} (μM)	MKN45 proliferation IC_{50} (μM)	sRON cell mech. IC_{50} (μM) ¹⁴
5a	0.086	0.56	0.57	0.13

nates, or sulfamide to afford compounds **5x–ab** and **6**. Hydrogenation of **5u** gave the piperidine analog **5v**. In addition, carboxyl derivatives could also be prepared, exemplified by the synthesis of the amide **5w** from (*R*)-**13a** by palladium-catalyzed carbonylation with CO gas in methanol, hydrolysis of the resulting methyl ester to the acid, and amide formation with methylamine.

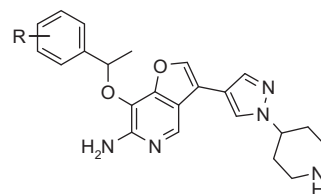
While the route outlined in Scheme 2 allowed rapid exploration of the C3 substituent, the R^1 substituent was introduced fairly early. Therefore, an alternative synthesis was used for the exploration of R^1 that took advantage of the advanced intermediate **12a** (Scheme 3). After Suzuki coupling with boronate **14**, the 1-(2,6-dichloro-3-fluorophenyl)ethyl moiety was removed cleanly with 48% aq HBr. Reprotecting the piperidine nitrogen as Boc carbamate gave the key intermediate **16**. Using similar conditions as for the corresponding steps in the other route, **16** was reacted with the alcohols **10** via Mitsunobu reaction, followed by reduction of the nitro group and removal of the Boc group to give the final compounds **5**.

The benzylic alcohols **10** were prepared from the corresponding aldehydes **17** by addition of the Grignard reagents $R^5\text{MgBr}$ or $R^5\text{MgCl}$ or by reduction of the acetophenones **18** with NaBH_4 (Scheme 4). The racemic mixtures were separated into the enantiomers either at the alcohol stage or as final compound.

Initial proof-of-concept efforts targeted the direct furopyridine analog **5a** of compound **2** (Table 1). This racemic compound showed sub- μM cellular activity against cMET and sRON, as well as good metabolic stability as measured by extraction ratios (ERs) of 0.47 and 0.30 in mouse and human liver microsomes, respectively, and was considered a viable starting point. Its 1-(piperidin-4-yl)-1*H*-pyrazolo-4-yl moiety was chosen as C3 substituent group for SAR exploration and optimization of the R^1 group, focusing on cellular potency against cMET.

Data for exploration of the substitution pattern of the phenyl ring in R^1 are shown in Table 2. The 3-fluoro substituent was important, as removing it (**5b**) or replacing it with a chloro (**5e**) or methoxy (**5f**) group resulted in less potent compounds. An additional fluorine at the 5-position (**5g**) improved the cMET biochemical potency; however, this improvement did not translate to the cellular context. Removing either of the *ortho*-chloro substituents (**5c**, **5d**) imparted a 3- to 11-fold potency loss, while replacing the 6-chloro with a bromo group (**5h**) retained cMET potency. Incorporating a chloro substituent at C-4 did not improve the

Table 2
SAR of the phenyl ring in R^1

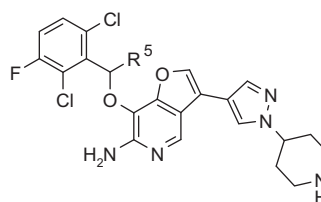


Compd ^a	R	cMET biochem. IC_{50} (μM)	MKN45 prolif. IC_{50} (μM)
5a	2,6-Di-Cl-3-F	0.086	0.57
5b	2,6-Di-Cl	0.22	2.0
5c	6-Cl-3-F	0.29	6.4
5d	2-Cl-3-F	0.36	5.1
5e	2,3,6-Tri-Cl	0.11	1.3
5f^b	2,6-Di-Cl-3-MeO	0.33	1.6
5g	2,6-Di-Cl-3,5-di-F	0.042	0.48
5h	2-Cl-3-F-6-Br	0.089	0.51
5i	2,4,6-tri-Cl	0.13	3.6

^a All compounds are racemic except for **5f** [(*R*) enantiomer].

^b Prepared from Boc-protected (*R*)-**5a** by treatment with sodium methoxide in DMSO followed by removal of the Boc group.

Table 3
SAR of the benzylic position R^5 in R^1



Compd	R^5	cMET biochem IC_{50} (μM)	cMET cell mech. IC_{50} (μM)	MKN45 prolif. IC_{50} (μM)
(<i>R</i>)- 5a	(<i>R</i>)- CH_3	0.047	0.41	0.30
(<i>S</i>)- 5a	(<i>S</i>)- CH_3	0.66	7.4	4.5
5j	H	0.43	>10	8.6
5k	<i>rac</i> -Et	0.092	2.2	3.6
5l	<i>rac</i> - <i>n</i> Pr	0.13	Not det.	2.7
5m	<i>rac</i> -Allyl	0.11	2.1	Not det.
5n	<i>rac</i> -Propargyl	0.070	0.56	0.36

potency (**5i** vs **5b**). While **5a**, **5g**, and **5h** were comparable in cMET potency, the substitution pattern of **5a** was preferred because of its lower molecular weight and better synthetic accessibility and was therefore held constant during further optimization.

Table 3 shows the SAR at the benzylic position in R^1 . The (*R*)-methyl substitution was preferred over its (*S*) enantiomer by 14- to 20-fold [(*R*)-**5a** vs (*S*)-**5a**]. The methyl group proved to be superior in terms of potency to hydrogen (**5j**), other alkyl groups (**5k–5l**), or allyl (**5m**), especially at the cellular level. While a propargyl group (**5n**) had comparable cMET potency to a methyl group, the compound showed significantly increased inhibition of CYP3A4 (IC_{50} : (*R*)-**5a**, >20 μM ; **5n**, 1.6 μM) and was therefore deprioritized. Based on this exploration, the 2,6-di-chloro-3-fluoro substitution pattern on the phenyl ring and (*R*)- CH_3 substitution at the benzylic position in R^1 were preferred.¹⁹

An X-ray structure of (*R*)-**5a** bound to cMET confirmed the expected binding mode with the amino acid backbone of the hinge region (Fig. 2): the 6-amino group interacts with the backbone carbonyl of Pro1158, and the core nitrogen forms a hydrogen bond

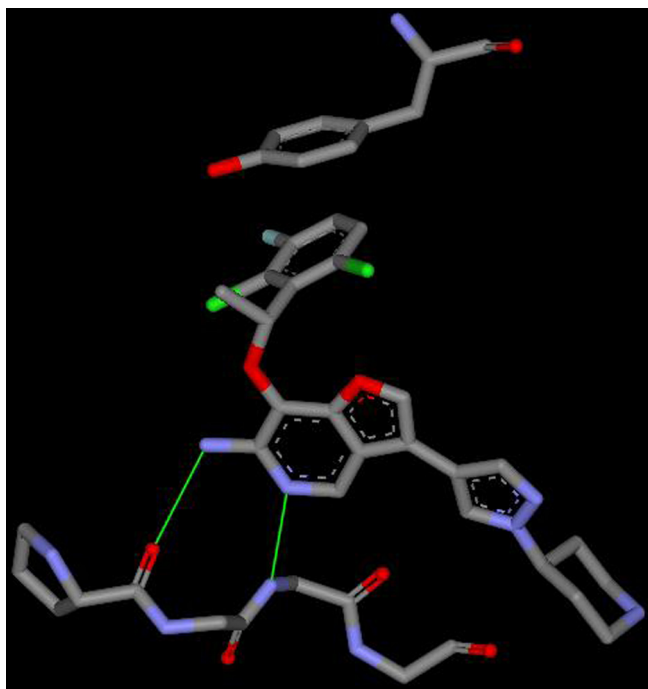


Figure 2. X-ray structure of (*R*)-**5a**/cMET (PDB code 4KNB). Shown are Tyr1230 from the activation loop and the backbone of the residues in the hinge region (Pro1158, Tyr1159, Met1160, Lys1161).

Table 4
Mouse PK data for (*R*)-**5a**^a

iv Dosing		<i>po</i> Dosing ^b	
Dose (mg/kg)	2	Dose (mg/kg)	20
V_{ss} (L/kg)	12	C_{max} (μ M)	0.15
Cl (mL/min/kg)	227	AUC _{0-last} (ng h/mL)	509
$t_{1/2}$ (h)	0.6	%F	35

^a PK parameters calculated by non-compartmental modeling using the median concentration at each timepoint (three animals per timepoint).

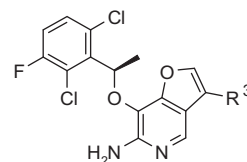
^b Dosed as solution of bis-HCl salt in 1:1 PEG400-water.

with the backbone NH of Met1160.²⁰ In addition, the 2,6-dichloro-3-fluorophenyl ring stacks tightly against the phenyl ring of Tyr1230 from the activation loop with a closest distance of 3.26 Å. Based on the structure, the improved potency of the 3-fluoro compound **5a** compared to **5b**, **5e**, or **5f** may be explained by a strengthened π - π interaction with the Tyr1230 phenyl ring, an enhanced pseudo H-bond between the adjacent CH and the carbonyl of Arg1208 (distance 3.78 Å), and by direct interactions with the β -carbon of Ala1221, the sulfur of Met1211, and the γ -carbon of Met1211 (distances 3.48–3.73 Å).

Compound (*R*)-**5a**, emerging as the best compound from this first round of optimization, showed metabolic stability as measured by extraction ratios (ERs) of ≤ 0.7 in both mouse and human liver microsomes (human, 0.56; mouse, 0.19) and was progressed to single-dose PK in female CD-1 mice. Very high clearance and high volume of distribution indicated extensive tissue distribution, resulting in low plasma levels and a short iv half-life. In addition, the overall exposure was low (Table 4). No significant metabolites were identified in plasma samples, indicating that the low exposure and rapid clearance were likely not due to metabolic liabilities.

With the R^1 substituent considered optimized, efforts shifted to the R^3 moiety to improve the pharmacokinetic properties of this series, as this group entered into the solvent-exposed region. It

Table 5
SAR of the R^3 substituent



Compd ^a	R^3	cMET biochem IC ₅₀ (μ M)	MKN45 proliferation IC ₅₀ (μ M)
(<i>R</i>)- 5a		0.047	0.30
5o		0.95	0.67
5p	Pyrazol-4-yl	0.19	3.3
5q	Phenyl	0.59	11
5r	Pyridin-2-yl	1.6	4.6
5s	Pyridin-3-yl	0.52	2.7
5t	Pyridin-4-yl	0.26	0.90
5u		0.030	0.45
5v		0.20	3.1
5w	CONHCH ₃	0.59	3.5
5x		0.32	0.33
5y		0.78	0.85
5z		0.58	0.51
5aa		0.28	0.19
6		0.14	0.13
5ab		1.0	0.55 ^b

^a All compounds are the (*R*) enantiomers.

^b cMET mechanistic IC₅₀.

was suspected that the high basicity of the piperidyl moiety in (*R*)-**5a**, while beneficial for solubility, might contribute to the high clearance and V_{ss} as well as low permeability (as indicated by the PAMPA assay). Thus, the emphasis was placed on compounds with reduced basicity (Table 5).

Acetylation of the piperidine (compound **5o**) improved the permeability (PAMPA: P_e at pH 7.4 = 318×10^{-6} cm/s) but also decreased the potency. Similar results were obtained with urea, carbamate, and sulfonamide analogs (data not shown). Additionally, the molecular weight of these analogs was >500 , a less desirable feature. Rather than further modifying the piperidine ring, we truncated the R^3 substituent and explored various proximal rings (compounds **5p–5v**). Among those, the tetrahydropyridine analog **5u** stood out in terms of potency. The corresponding piperidine **5v** was about sevenfold less potent, indicating that planarity with the furopyridine core was important. A set of amides, represented by **5w**, was also prepared that aimed to form a hydrogen bond

Table 6
Rodent PK of **6** (OSI-296)^a

6 (OSI-296)	Mouse	Rat
<i>iv</i> Dosing		
Dose (mg/kg)	2	2
Cl (mL/min/kg)	51	39
V_{ss} (L/kg)	3.8	6.8
$t_{1/2}$ (h)	2.9	2.0
<i>po</i> Dosing		
Dose (mg/kg)	20	20
Salt form	Mesylate salt ^b	Free base ^b
C_{max} (μ M)	4.8	2.5
AUC _{0–last} (ng h/mL)	5425	6204
%F	83	72

^a PK parameters calculated by non-compartmental modeling using the median concentration at each timepoint (three animals per timepoint).

^b Both formulated as solution in 40% HPCD in 0.01 M HCl.

Table 7
Selectivity data for **6** (OSI-296)^a

Kinase	IC ₅₀ (μ M)	Kinase	IC ₅₀ (μ M)
cMET biochem.	0.026	ALK biochem.	0.040
cMET Y1230C	0.072	ALK cell mech.	0.50
cMET Y1230H	0.11	KDR biochem.	1.3
cMET cell mech.	0.042	KDR cell mech.	6.1
cMET mech. + mp ^b	0.60	AurB biochem.	0.011
RON biochem.	0.025	AurB cell mech.	1.0
sfRON cell mech.	0.20	AurB mech. + mp ^b	>10

^a Cell mechanistic assays monitored the autophosphorylation sites of cMET (MKN45), RON (HeLa-sfRON), ALK (Karpas-299), and KDR (HUVEC) or p-Ser10 of histone H3 for Aurora B (HT-29). Biochemical IC₅₀ values were determined using the Invitrogen Omnia format at an ATP concentration equal to K_m .

^b Cell mechanistic assay in the presence of 50% mouse plasma.

from the amide NH with the hinge backbone carbonyl of Met1160. However, sub-micromolar cellular potencies could not be achieved with these compounds.

From among these proximal rings, the tetrahydropyridine was selected for further optimization (compounds **5x–5ab**, **6**). Gratifyingly, cellular potency was retained upon acetylation (**5x**), and the PAMPA assay indicated good permeability (P_e at pH 7.4 = 199×10^{-6} cm/s). While the carbamate **5v** and dimethylurea **5z** had reduced potencies, the methyl urea **5aa** and primary urea **6** showed comparable or better cell potencies than (*R*)-**5a**. Based on the structural information, this may be explained by a hydrogen bond between the urea NH and the backbone carbonyl of Lys1161 at the tip of the hinge region. The sulfamide analog **5ab**, in contrast, was less potent.

Compound **6** (OSI-296) met the *in vitro* criteria of cellular cMET potencies equal to or better than (*R*)-**5a**, significant permeability in the PAMPA assay (P_e at pH 7.4 = 359×10^{-6} cm/s), and metabolic stability as measured by extraction ratios (ERs) of 0.7 in both mouse and human liver microsomes and was progressed to single-dose mouse PK. It showed a significantly improved PK profile compared to (*R*)-**5a**, achieving a C_{max} of 2.4 μ M with moderate clearance and good oral exposure when dosed as an HCl salt in PEG400/water. With an optimized formulation suitable for repeat dosing in efficacy and toxicology studies [methanesulfonate (mesylate) salt of **6** in 40% w/v HPCD (Trappsol®) in 0.01 M HCl], C_{max} , oral exposure, and bioavailability were further improved (Table 6). Good PK was also observed in female Sprague–Dawley rats. The high solubility of **6** at low pH (pH 3, >100 μ M; pH 4.5, 11 μ M) decreased to approx. 1 μ M around physiological pH.

Biochemical and cellular IC₅₀ values are summarized in Table 7. Compound **6** showed potent inhibition of cMET and RON in biochemical and cellular assays with submicromolar activity against

cMET in the presence of mouse plasma.²¹ The biochemical potency against two cMET Y1230 mutants was reduced by 3–4 \times compared to wild-type cMET.²² To establish the biochemical selectivity profile, **6** was tested against a panel of 96 kinases.²³ Besides cMET, Aurora, Arg, and Abl were the only kinases that showed >50% inhibition at 1 μ M of **6**; RON was not present in this screening panel. The potent biochemical Aurora B activity in that assay did not translate to the cellular setting with a mechanistic IC₅₀ in the presence of mouse plasma of >10 μ M; in addition, **6** had no significant impact on ploidy in a FACS assay up to 10 μ M.²⁴ It showed minimal activity against KDR in biochemical and cellular assays, thus achieving differentiation from cMET/KDR inhibitors such as XL880 and XL184.⁸ Compound **6** was less potent against ALK than against cMET and RON and showed no significant activity in the ALK-driven Karpas-299 xenograft model at doses of up to 200 mg/kg qd.²⁵ While **6** inhibited proliferation of cMET-driven cell lines such as MKN45 at concentrations near the respective cell mechanistic IC₅₀, no antiproliferative activity was observed in non-driven lines, for example, HCT-116 and MDA-MB-231 (IC₅₀ >2 μ M). This indicates that the antiproliferative effects of **6** are based on inhibition of the intended targets and not general cytotoxicity. Thus, OSI-296 (**6**) is best described as a selective cMET/ RON inhibitor.

The favorable pharmacokinetic profile displayed by **6** in the mouse, with good exposure and oral bioavailability, led to its evaluation in pharmacodynamic and efficacy studies.

Pharmacodynamic (PD) studies were performed in the MKN45 xenograft model, evaluating effects on phosphorylation of the cMET receptor in relation to plasma drug levels.

Following a 100 mg/kg single oral dose of **6**, a >80% sustained inhibition of MET auto-phosphorylation (pY1234/1235) was observed up to 8 h, corresponding to plasma levels of >3 μ M. This correlated with the plasma concentration being above the cMET mech. + mouse plasma IC₅₀ value for the entire 8 h time period. Drug levels dropped to 0.52 μ M by 16 h, with slow recovery of pMET content (45% inhibition at 24 h) (Fig. 3). Similar effects were observed for pY1349 cMET (site essential for creating docking site for downstream signaling; data not shown).

The *in vivo* efficacy of **6** dosed orally on a once-daily schedule for 14 days was initially evaluated in the MKN45 xenograft model in female nu/nu CD-1 mice (Fig. 4). The compound exhibited a clear dose response, showing an ED₅₀ of 50 mg/kg and reaching 100% tumor growth inhibition (TGI) with regressions (27%) at 100 mg/kg qd. Analysis of cMET pY1234/1235 phosphorylation status in tumor samples collected at the end of dosing indicated that >90% inhibition of pMET for 24 h correlated with complete inhibition

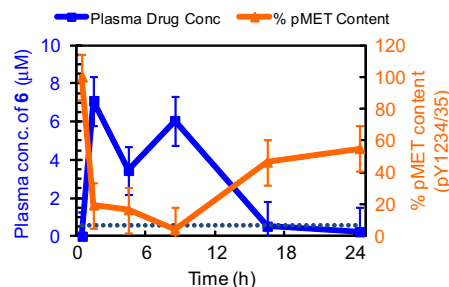


Figure 3. Correlation of inhibition of cMET phosphorylation and plasma drug exposure in MKN45 tumor xenografts following oral dosing with **6** (OSI-296). The blue line corresponds to median plasma concentrations of **6** at indicated time following a 100 mg/kg qd dose. The orange line represents median pMET (pY1234/1235) content normalized with total cMET in MKN45 tumors and expressed as a percentage of control pMET content from vehicle-treated animals. The dotted blue line indicates the cMET cell mechanistic IC₅₀ in the presence of mouse plasma (0.60 μ M).

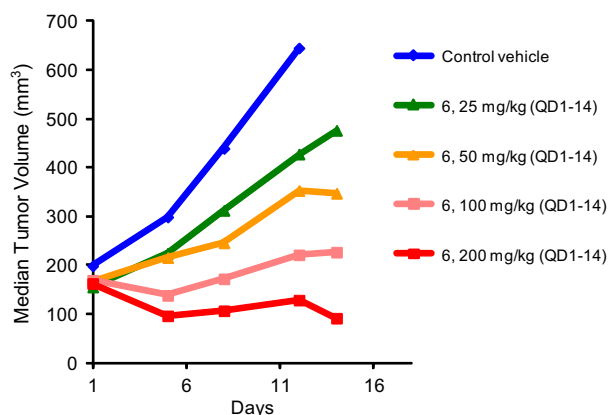


Figure 4. Tumor growth inhibition (TGI) data for **6** (OSI-296) in MKN45 tumor xenografts. The compound was dosed orally as mesylate salt in 40% HPCD in 0.01 M HCl.

Table 8
In vivo efficacy data for **6** (OSI-296)

Tumor line	Dose and schedule	Avg.% TGI	Max.% regression	% BWL
MKN45 ^a	25 mg/kg qd (1–14)	13	0	6
	50 mg/kg qd (1–14)	51	0	2
	100 mg/kg qd (1–14)	100	27	3
	200 mg/kg qd (1–14)	100	49	3
SNU-5 ^b	50 mg/kg qd (1–20)	100	31	4
	100 mg/kg qd (1–20)	100	64	2
	200 mg/kg qd (1–20)	100	80	4
U87MG ^b	50 mg/kg qd (1–14)	58	0	0
	100 mg/kg qd (1–14)	79	0	0
	200 mg/kg qd (1–14)	94	8	0
	50 mg/kg bid (1–14)	79	0	5
	100 mg/kg bid (1–14)	97	22	0

^a Dosed as solution of mesylate salt in 40% HPCD in 0.01 M HCl.

^b Dosed as solution of free base in 60:40 PEG400/25 mM tartaric acid.

of tumor growth (100% TGI). Significant tumor growth inhibition was also observed in other cMET-driven models such as SNU-5 (gastric carcinoma) and U87MG (glioblastoma). The study in the U87MG model also compared dosing on a once-daily versus twice-daily schedule. The data suggest that for this model there is no advantage in administration of **6** as two divided doses compared to a cumulative dose on a once-daily schedule. In all models, the compound was very well tolerated with minimal body weight loss (BWL; 0–6%), even at the highest doses of 200 mg/kg qd and 100 mg/kg bid (Table 8).

The potential for mutagenicity of **6** was evaluated in an Ames test using the TA98 and TA100 strains; it was negative for the induction of reverse mutations with and without an S9 metabolic activation system.

In summary, we designed and synthesized 6-aminofuro[3,2-c]pyridines **5** and demonstrated their usefulness as kinase inhibitors by optimizing this series towards inhibition of cMET and RON, leading to OSI-296 (**6**). This compound exhibited selectivity in a panel of 96 kinases with potent activity against cMET, including common Y1230 mutants, and RON. OSI-296 showed a PK profile in rodents suitable for oral dosing with >70% bioavailability. In multiple cMET-driven xenograft models in mice, significant tumor growth inhibition was observed at once-daily doses of 50 mg/kg or less, with regression at higher doses. OSI-296 was very well tolerated with little body weight loss and no adverse effect even at the highest tested dose of 200 mg/kg po once-daily. A PK/PD/TGI correlation has been established wherein >90% inhibition of cMET phosphorylation sustained over 24 h by OSI-296 dosed at 100 mg/kg po

once-daily translated to 100% TGI. The compound was negative in the Ames test. Its overall activity profile as cMET/RON inhibitor differentiates it from cMET/KDR inhibitors, such as XL880 and XL184, and from the ALK/cMET inhibitor Crizotinib (**2**).²⁶ Taken together, these data supported further evaluation of OSI-296 in RON-driven models, which will be detailed in subsequent publications.

Acknowledgments

We would like to thank Ms. Viorica M. Lazarescu and Dr. Yingjie Li for analytical support and Mr. Paul Maresca, Mr. Peter Meyn, Ms. Brianna Tokar, Dr. Earl May, and Dr. Brenda Petronella for conducting in vitro ADMET studies and kinase selectivity profiling.

Supplementary data

Supplementary data (detailed procedures of MKN45 proliferation, cMET and sFRON cell mechanistic, and cMET biochemical assays; descriptions of metabolic stability, CYP3A4, and PAMPA assays; SAR at the 2-position of the furo[3,2-c]pyridine core; waterfall plot of biochemical kinase selectivity data; analytical data for compound **6** as free base and mesylate) associated with this article can be found, in the online version, at <http://dx.doi.org/10.1016/j.bmcl.2013.05.074>.

References and notes

- (a) Cui, J.; Tran-Dubé, M.; Shen, H.; Nambu, M.; Kung, P.-P.; Pairish, M.; Lei, J.; Meng, J.; Funk, L.; Botrous, L.; McTigue, M. A.; Grodsky, N.; Ryan, K.; Padriquet, A.; Alton, G.; Timofeevski, S. L.; Yamazaki, S.; Li, Q.; Zou, H. Y.; Christensen, J. G.; Mroczkowski, B.; Bender, S.; Kania, R. S.; Edwards, M. P. *J. Med. Chem.* **2011**, *54*, 6342; (b) Rodig, S. J.; Shapiro, G. I. *Curr. Opin. Investig. Drugs* **2010**, *11*, 1477.
- Barlaam, B. C.; Bower, J. F.; Delouvie, B.; Fairley, G.; Harris, C. S.; Lambert, C.; Ouvry, G.; Winter, J. J. G. WO 2009/053737; *Chem. Abstr.* **2009**, *150*, 472757.
- Hilton, S.; Naud, S.; Caldwell, J. J.; Boxall, K.; Burns, S.; Anderson, V. E.; Antoni, L.; Allen, C. E.; Pearl, L. H.; Oliver, A. W.; Aherne, G. W.; Garrett, M. D.; Collins, I. *Bioorg. Med. Chem.* **2010**, *18*, 707.
- Ghose, A. K.; Herberich, T.; Pippin, D. A.; Salvino, J. M.; Mallamo, J. P. *J. Med. Chem.* **2008**, *51*, 5149.
- This binding mode has been confirmed for **2** by crystallography of a complex with cMET; see: Timofeevski, S. L.; McTigue, M. A.; Ryan, K.; Cui, J.; Zou, H. Y.; Zhu, J. X.; Chau, F.; Alton, G.; Karlicek, S.; Christensen, J. G.; Murray, B. W. *Biochemistry* **2009**, *48*, 5339.
- Maggiara, P.; Gambarotta, G.; Olivero, M.; Giordano, S.; Di Renzo, M. F.; Comoglio, P. M. *J. Cell Physiol.* **1997**, *173*, 183.
- Comoglio, P. M.; Giordano, S.; Trusolino, L. *Nat. Rev. Drug Disc.* **2008**, *7*, 504.
- Eder, J. P.; Vande Woude, G. F.; Boerner, S. A.; LoRusso, P. M. *Clin. Cancer Res.* **2009**, *15*, 2207.
- Wang, M. H.; Wang, D.; Chen, Y. Q. *Carcinogenesis* **2003**, *24*, 1291.
- Angeloni, D.; Danilkovitch-Miagkova, A.; Ivanova, T.; Braga, E.; Zabarovsky, E.; Lerman, M. I. *Oncogene* **2007**, *26*, 4499.
- Smolen, G. A.; Sordella, R.; Muir, B.; Mohapatra, G.; Barmettler, A.; Archibald, H.; Kim, W. J.; Okimoto, R. A.; Bell, D. W.; Sgroi, D. C.; Christensen, J. G.; Settleman, J.; Haber, D. A. *Proc. Natl. Acad. Sci. U.S.A.* **2006**, *103*, 2316.
- MKN45 proliferation assay: 3-day incubation, Cell Titer-Glo used for readout. For details, please see the Supplementary data.
- cMET cell mechanistic assay: MKN45 cells, phosphorylated MET levels measured by incubating with a rabbit polyclonal antibody against MET [pYpY1230/1234/1235] followed by an anti-rabbit antibody conjugated to HRP. For details, please see the Supplementary data.
- Under the assay conditions used herein, the IC₅₀ values between the MKN45 proliferation and cMET cell mechanistic assays correlated nearly 1:1.
- sFRON cell mechanistic assay: HeLa cells transfected with sFRON-pcDNA, phosphorylated RON levels measured by incubating with a goat polyclonal antibody against phosphorylated RON (pYpY1238/1239) followed by an anti-goat antibody conjugated to HRP. For details, please see the Supplementary data.
- Eloy, F.; Deryckere, A. *Helv. Chim. Acta* **1970**, *53*, 645.
- Engler, T. A.; Malhotra, S.; Burkholder, T. P.; Henry, J. R.; Mendel, D.; Porter, W. J.; Furness, K.; Diefenbacher, C.; Marquart, A.; Reel, J. K.; Li, Y.; Clayton, J.; Cunningham, B.; McLean, J.; O'Toole, J. C.; Brozinick, J.; Hawkins, E.; Misener, E.; Briere, D.; Brier, R. A.; Wagner, J. R.; Campbell, R. M.; Anderson, B. D.; Vaughn, R.; Bennett, D. B.; Meier, T. I.; Cook, J. A. *Bioorg. Med. Chem. Lett.* **2005**, *15*, 899.
- cMET biochemical assay: AlphaScreen in 384-well plates using biotinylated poly(Glu, Tyr) as substrate. For details, please see the Supplementary data.
- We also briefly explored substitution at the 2-position of the furo[3,2-c]pyridine core. However, none of the synthesized compounds improved cMET potency compared to (R)-**5a** (please see Supplementary data, Table S1, for details).

20. Crystallographic information: resolution 2.40 Å, space group P21, four molecules in the asymmetric unit. Crystallization and solution of structure performed by Proteros Biostructures GmbH, Am Klopferspitz 19, D-82152, Martinsried, Germany, www.proteros.com. Crystallographic data for the structure have been deposited with the PDB (pdb code 4KNB).
21. In addition to the 'shift assays', the plasma protein binding of **6** was also determined by equilibrium dialysis (human plasma, 98.1% bound; mouse plasma, 98.2% bound).
22. The cMET inhibitors PF-04217903 and PF-02341066 (**2**) showed a biochemical potency loss against these two mutants of ≥ 600 -fold and 8- to 9-fold, respectively; see Ref.5
23. The mobility shift assay technology from Caliper LifeSciences (ProfilerPro™ Kinase Selectivity Assay Kits 1–4) was used.
24. Polyploidy is a phenotypic readout for inhibition of Aurora B, see for example: Ditchfield, C.; Johnson, V. L.; Tighe, A.; Ellston, R.; Haworth, C.; Johnson, T.; Mortlock, A.; Keen, N.; Taylor, S. S. *J. Cell. Biol.* **2003**, *161*, 267.
25. In contrast, Crizotinib (**2**) was reported to give 96% TGI at 50 mg/kg qd in this model, see: Christensen, J. G.; Zou, H. Y.; Arango, M. E.; Li, Q.; Lee, J. H.; McDonnell, S. R.; Yamazaki, S.; Alton, G. R.; Mroczkowski, B.; Los, G. *Mol. Cancer Ther.* **2007**, *6*, 3314.
26. Dussault, I.; Bellon, S. F. *Anticancer Agents Med. Chem.* **2009**, *9*, 221.